A WIND TUNNEL BASED STUDY OF THE FLOW FIELD BEHIND SAILPLANE WINGLETS

P.Anderle*, F.N.Coton**, L. Smrcek**, V. Broz*
* CTU in Prague, Dept. of Automotive and Aerospace Engineering, CZ.
** University of Glasgow, Dept. of Aerospace Engineering, Glasgow,UK

Keywords: *winglet, vorticity, hot-wire anemometry, downwash*

Abstract

This paper describes an experimental investigation of velocity and vorticity distributions in the flow field behind wing-tip devices. The objective of this work was to gain a greater understanding of how the wing-tip geometry modifies the vortex structure behind the wing. The research has involved examining the velocity and vorticity distribution in the flow field, using hot-wire anemometry. In order to carry out measurements with the hot-wire anemometry system, a new traverse mechanism was designed, manufactured and set-up. This traverse mechanism was integrated with other test instrumentation to create a complete measurement chain. The measurements were performed in the Handley-Page wind tunnel of the Aerospace Engineering Department at the University of Glasgow.

1 Introduction

The induced drag makes a significant contribution to the total drag and is a result of generating lift on a finite wing. Literature suggests that the induced drag accounts for around 70% of the total drag during climb, 25% during cruise and 40% during landing [1]. It is therefore reasonable to try to reduce the induced drag as a means of improving the aircraft performance.

The wing tip vortices on large aircraft can be so powerful as to endanger smaller aircraft flying behind them. The energy in the vortices can be modified through displacement or reduction. These modifications can potentially be achieved by the use of wing tip devices that can be categorized as either active or passive devices [2].

In the present context active devices are considered to incorporate moving parts and could, for example, take the form of wing tip turbines [3]. Wing tip propellers are also active devices, and have been proposed as a means to reduce induced drag [4].

Passive devices, on the other hand, have fixed geometries and usually take the form of modifications to the wing tip geometry. Wing tip modifications such as the cut wing tip or drooped wing tip are simple examples of this. These modifications work to change the location of the vortex core and, in so doing, increase the effective span of a wing, so reducing the induced drag. Other concepts to modify wing tip vorticity include wing tip sails and the WING-GRID [5], [6].

Beneficial effects have also been obtained by the addition of vertical surfaces such as end plates. In the late 1960s, designers began experimenting with wing-tip geometries using 'small' vertical extensions to reduce the formation of tip vortices but this concept actually dates back to 1897, when Frederick Lanchester took out a patent on the idea, incorporating it into some of his wing theories[7]. His wing had two 'capping planes' at the end of it, that became known in the 1920s as 'end plates', when Prandtl extended his basic lifting line concept[8].

The real break-through with winglets was made by Whitcomb. In 1976, he published a paper that compared a wing with a winglet and the same wing with a simple extension to increase its span[9]. Whitcomb showed that winglets reduced drag by about 20 percent and

increased the wing lift-drag ratio by approximately 9 percent. His design, which takes advantage of twist to get a component of the winglet's lift in the thrust direction, soon attracted the attention of the aviation industry.

Winglets are now being incorporated into most new commercial and military transport jets. Since the 1980s, most modern high performance sailplanes also have small vertical wing tip extensions.

The first sailplanes to have winglets were the ASW-20FP, GEMINI and NIMBUS 3. Sets of Whitcomb style winglets were fitted to these wings in the late 1980's. Flight tests carried out on these aircraft demonstrated the effect of winglets on high aspect ratio wings[10].

In this paper, two sailplane wing tip geometries are investigated in a low speed wind tunnel. The way in which the trailed vortical structures depend on the tip geometry will be demonstrated. The effect these have on the wing and winglet wake will also be examined and discussed.

2 Wing tip Vortex Formation

The air tends to flow from an area of high pressure to areas of lower pressure, when the wing passes through the air. The result of this pressure difference also gives rise to a secondary flow at the wing tip. The effect of this secondary flow is a deflection of the free stream, called outwash on the lower surface and inwash on the upper surface. This deflection of the air stream caused by the pressure difference, combined with the forward movement of the plane, produces a wingtip vortex. The vortex contains considerable energy in the form of a swirling flow.

This basic description of the flow holds regardless of whether the wing includes a winglet or not. The primary effect of the winglet is to alter the distribution of the vorticity at the wing tip.

3 Test Facilities

3.1 Wind Tunnel

The Handley Page wind tunnel is an atmospheric low-speed wind tunnel with a closed return circuit equipped with a rectangular test-section of dimensions 2.15m by 1.60m and of length 3.38m (Fig.1). A turntable, 0.97 metres in diameter, built into the test section floor can rotate the models. Several venting slots in the tunnel walls at the test section exit maintain near atmospheric static pressure. The nozzle placed in front of the test section has a contraction ratio of 4:1. The power supply is an electric motor that drives a fan 2.3 m in diameter to provide the airflow in the wind tunnel. The tunnel can reach speeds up to 60 m/s.
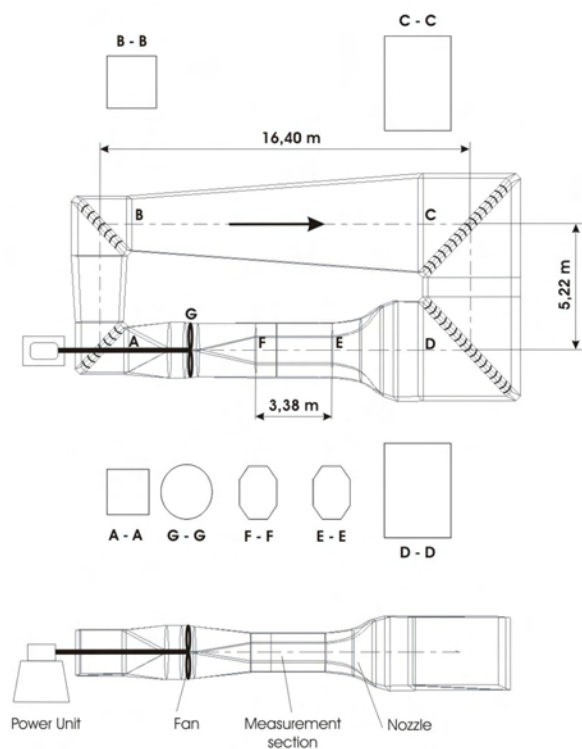
Fig. 1. Handley Page wind tunnel circuit

3.2 Wind Tunnel Models of Winglets

The wind tunnel models used in the experiments were real wing tips taken from the single seat, HpH 304CZ/C sailplane´s wings. During the experimental program several wing tip geometries were studied. In this paper two of

these are investigated; a standard HpH 304 wing without a winglet and the HpH 304 sailplane's detachable winglet.

The wing tip - model A (Fig.2) is basically a standard wing tip with a small vertical extension that projects downwards from the lower surface of the wing. This small extension protects the wing tip against damage during the sailplane's take-off and landing.

Fig. 2. Standard wing tip – model A

The leading edge of the detachable winglet – model B (Fig.3) has 30 degrees of sweep-back, a cant angle of 5 degrees and twist of 3 degrees.

There is also a small radius smoothing the transition between the wing and winglet.

Fig. 3. Detachable winglet – model B

3.3 Measurement Procedure

The measurement chain consisted of an x-wire sensor, a TSI IFA 300 constant temperature anemometry system, a personal computer, a SMOCI transmitter and a traversing mechanism as shown in Figure 4.

Fig. 4. Wind Tunnel Test Configuration

The X-wire sensor was connected to two channels of the IFA 300 by coaxial cables. The IFA 300 hardware converted the acquired signals from the sensors and transmitted them to the controlling computer via a BNC adapter block and data acquisition card. The IFA 300 software installed on the computer processed the recorded data. Once the data had been recorded for an entire Y traverse, a master program, written in LABView, sent a new instruction to the SMOCI unit. The SMOCI transmitter converted the instruction into the signal needed by the stepper motors to move the traverse to its next Z position. When the traverse mechanism reached this new position, another signal was sent to it to begin its Y traverse. The x-wire sensor continually sampled data during this traverse and sent the signals to the computer. This process continued until measurements had been made over the entire measurement grid.

The models were mounted upstream of the traverse on a base plate that was secured to a rail track mechanism as shown in Fig. 4. This mechanism allowed the model to be moved backwards and forwards in the wind tunnel working section to change the distance between the model and the hot-wire measurement plane. In addition, the base plate was designed to allow the incidence of the model to be changed.

A two component traverse capable of moving the probe to any point within a 850 mm x 930 mm grid was used during the experiments. It was mounted behind the test models such that measurements could be made in planes perpendicular to the onset flow. The location of the measurement plane with respect to the test model could be varied using the model mounting tracks described above. The horizontal motion was provided by a large, off-the-shelf linear slide driven by a stepper motor. Vertical movement was provided by a purpose built traverse mechanism based on a precision ball screw. The incremental resolution of the linear motion was 0.03 mm.

4 Experimental Results

In this section measurements of the three-dimensional vortex systems behind the two wing tip models will be presented for a range of incidences and downstream distances.

4.1 Vortex Structures

The vortex structures were examined by measuring the U, V and W velocity components in 3 planes perpendicular to the wind tunnel axis (x/b=0.2, x/b=1, x/b=2, where x is the distance behind the wing tip and b is the wing chord) with the wing at the angles of attack α= 0, 3 and 6 degrees at a free stream velocity U=33 m/s.

The vorticity field was calculated directly from the measured velocity field. Figure 5 shows the rectangular coordinate system used for the measurement of the 3-dimensional velocity field, with $+X$ in the direction of the freestream flow, $+Y$ normal to the plane of the wing, and $+Z$ in the direction of the span of the wing.

$$\omega_x = \frac{\partial V}{\partial z} - \frac{\partial W}{\partial y} \qquad (1)$$

Equation (1) defines the vorticity component in the X direction (streamwise vorticity), where V and W are the velocity components in the Y and Z directions respectively.
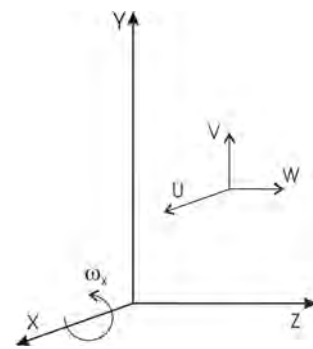
Fig. 5. Coordinate system and velocity components

Figures 6 and 7 present examples of velocity and vorticity data measured for wing tip model A and wing tip model B in the three measurement planes at an angle of attack of 6 degrees.
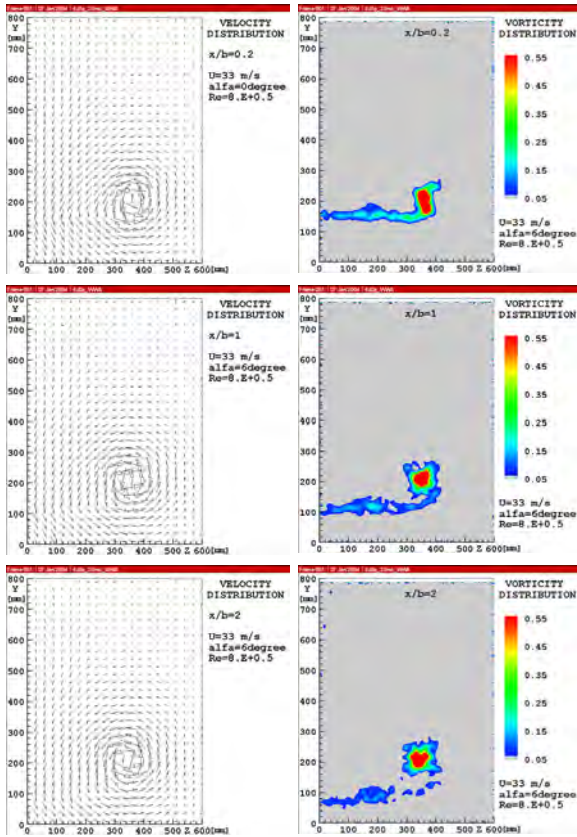
Fig. 6. Velocity and vorticity distribution at three distances downstream of wing tip model A (α=6°)

4.2 Downstream Wake Position

Figures 8 and 9 give the location of the downstream wakes behind the two models (i.e. the regions of the flow containing decelerated particles that have passed through the boundary layer). The regions were identified from the matrices of measured points by suppressing velocities of the free stream value or higher.
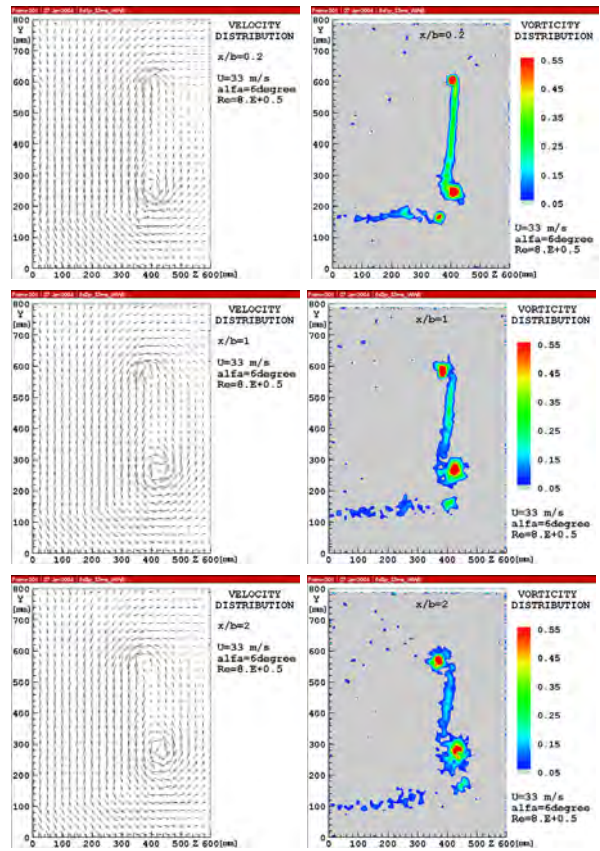
Fig. 7. Velocity and vorticity distribution at three distances downstream of wing tip model B (α=6°)
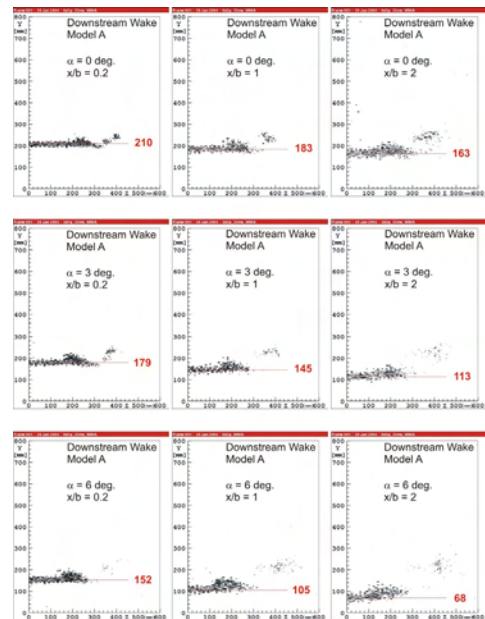
Fig. 8. Wake formation at three distances downstream of wing tip model A (α=0°,3° & 6°)
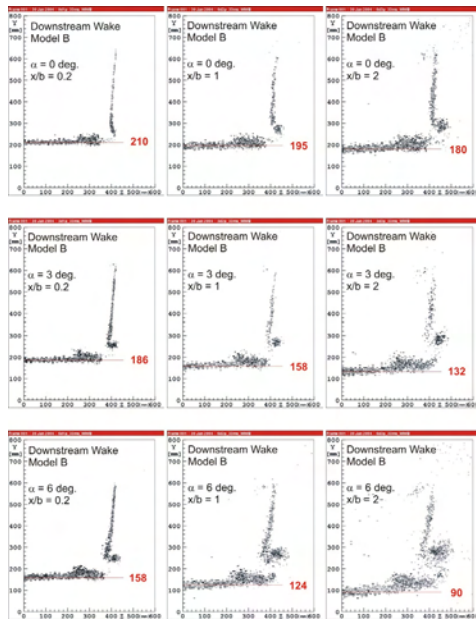
Fig. 9. Wake formation at three distances downstream of wing tip model B (α=0°,3° & 6°)

4.3 Discussion of Experimental Results

4.3.1 Wing tip Model A
Wing tip model A produces an almost classical tip vortex structure where the vorticity is concentrated in a single structure that rolls up slightly inboard of the wing tip (Fig. 6). Also visible in Fig. 6. is the vorticity in the wake of the main wing. The tip vortex strength increases with increasing angle of attack and also, as is apparent in Fig. 6, with distance downstream of the wing tip. Conversely, the vorticity level in the wake gradually decays when moving downstream. This behaviour is consistent with the progressive concentration of vorticity in the tip vortex during the roll-up process.

Another interesting feature of Fig. 6 is the progressive downward deflection of the wake under the influence of the downwash from the tip vortex. This is also visible in Fig. 8 which also illustrates that the magnitude of the downward deflection depends on the wing incidence i.e. the greater the incidence, the stronger the tip vortex and the greater the downward deflection of the wake.

4.3.2 Winglet Model B
In this case, there are two clear separated vortex structures: One at the wing/winglet junction and the other at the tip of the winglet (Fig. 7). The results show the roll-up process during which the vortex core produced at the wing/winglet junction moves outboard and the winglet tip vortex moves inboard. These two vortical structures are connected by a vortex sheet that is initially vertically aligned. The strength of this vortex sheet depends on the cant angle of the winglet, its twist distribution and the onset flow angle. With increasing downstream distance this vortex sheet gradually decays and deflects in the direction of rotation of the global vortex system. When compared to wing tip model A, the vorticity in the wake of the main wing is almost non-existent. This is interesting because, as shown in Figs 8 and 9, the velocity deficit in this region is similar for the two wing tip geometries. Clearly, however, the wake from wing tip model A is deflected further downwards in comparison to that of model B. This indicates that the wing tip geometry has a strong impact on the distribution of induced velocity around the wing tip.

4.4 Analysis of the Vorticity Distribution
This section describes analysis of the measured velocity fields to extract the circulation strength of the wing tip vortex system.

4.4.1 Definition of Circulation
The circulation is defined as:

$$\Gamma = \oint_C \mathbf{u} \cdot d\mathbf{l} \qquad (2)$$

where the line integral is taken along a closed contour C that encloses the region of interest. Figure 10 illustrates the calculation of circulation in the YZ plane behind the wing tip models based on this equation.
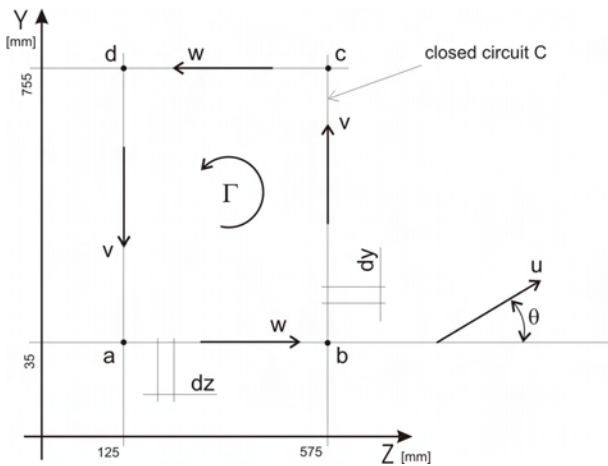
Fig. 10. Definition of circulation in the YZ plane behind the wing tip models

On this basis it is possible to express the circulation equation as

$$\Gamma = \oint_C \mathbf{u} \circ \mathbf{dl} = \oint_C \mathbf{u} \cdot \cos \theta \, \mathbf{dl} \qquad (3)$$

where the expression $u.\cos \theta$ is equal either to the vectors V or W measured by the x-wire probe.

4.4.2 Calculation of Circulation

The circulation magnitudes calculated by the procedure described in the previous section are presented in Tables 1 and 2 for wing tip models A and B respectively. The data contained in the tables are for a series of integration paths around the vortex systems. These are shown in Figs. 11 and 12. The obvious requirement for the choice of the integration path is that the path contains all the significant vorticity in the downstream measurement plane. If this condition is satisfied, the magnitude of the circulation should be constant regardless of the path of integration.

Tables 1 and 2 give the calculated values for particular contours, the average values and the deviation from the average. All calculated values fall within 5% of the appropriate average confirming that the measurement domain is sufficient to fully capture the vortex structures produced by the wing tips.
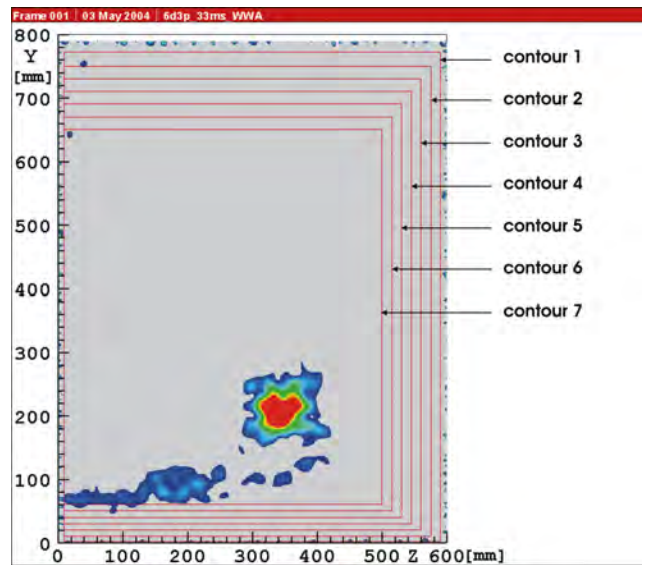
Fig. 11. Definition of integration paths-model A

deg.	1 plane		2 plane		3 plane	
	Γ [m²/s] *					
0	3161		2900		2862	
3	3902		3829		3815	
6	4877		4853		4807	
		[%]**		[%*]*		[%]**
contour 1:	0	3184	1	2870	1	2892	1
contour 2:		3180	1	2896	0	2778	3
contour 3:		3184	1	2924	1	2875	0
contour 4:		3183	1	2872	1	2855	0
contour 5:		3200	1	2900	0	2858	0
contour 6:		3099	2	2989	3	2877	1
contour 7:		3100	2	2851	2	2900	1
contour 1:	3	3887	0	3845	0	3830	0
contour 2:		3877	1	3710	3	3722	2
contour 3:		3834	2	3873	1	3832	0
contour 4:		3966	2	3797	1	3824	0
contour 5:		3881	1	3771	2	3761	1
contour 6:		4010	3	3932	3	3841	1
contour 7:		3860	1	3877	1	3893	2
contour 1:	6	4881	0	4876	0	4788	0
contour 2:		4749	3	4763	2	4711	2
contour 3:		4918	1	4870	0	4847	1
contour 4:		4876	0	4873	0	4804	0
contour 5:		4892	0	4857	0	4870	1
contour 6:		4883	0	4846	0	4868	1
contour 7:		4940	1	4886	1	4762	1

Table 1. Dependence of the circulation magnitude on integration path - model A (* average values, ** % deviation from average)
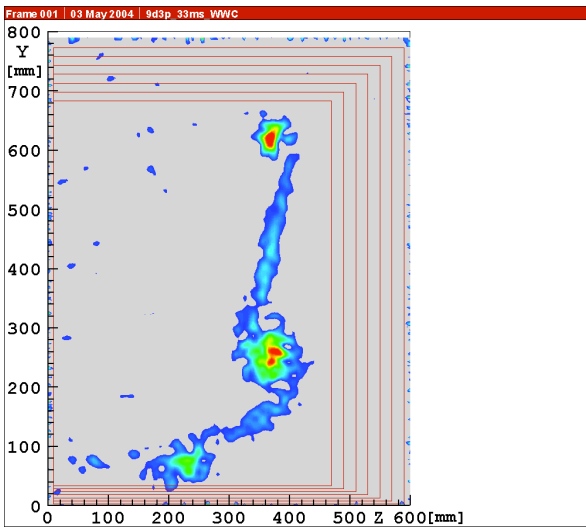
Fig. 12. Definition of integration paths-model B

	deg.	1 plane		2 plane		3 plane	
		Γ [m²/s] *					
	0	2792		2774		2757	
	3	4308		4263		4122	
	6	5067		5024		4858	
		[%]**		[%]**		[%]**	
Contour 1:	**0**	2808	1	2798	1	2803	2
Contour 2:		2661	5	2754	1	2660	4
Contour 3:		2826	1	2828	2	2703	2
Contour 4:		2779	0	2833	2	2808	2
Contour 5:		2824	1	2716	2	2806	2
Contour 6:		2773	1	2692	3	2763	0
Contour 7:		2871	3	2795	1	2757	0
Contour 1:	**3**	4280	1	4272	0	4035	2
Contour 2:		4124	4	4226	1	4002	3
Contour 3:		4350	1	4201	1	4173	1
Contour 4:		4394	2	4294	1	4041	2
Contour 5:		4363	1	4329	2	4181	1
Contour 6:		4248	1	4276	0	4230	3
Contour 7:		4396	2	4246	0	4195	2
Contour 1:	**6**	4990	2	5010	0	4801	1
Contour 2:		4934	3	4916	2	4751	2
Contour 3:		5052	0	5058	1	4907	1
Contour 4:		5053	0	5106	2	4883	1
Contour 5:		5115	1	5036	0	4844	0
Contour 6:		5125	1	4998	1	4888	1
Contour 7:		5200	3	5042	0	4932	2

Table 2. Dependence of the circulation magnitude on integration path- model B(* average values, ** % deviation from average)

The data presented in Tables 1 and 2 show some consistent trends such as the increase in circulation strength with increasing angle of attack in both cases. Comparison of the data in the two tables, however, shows that the effect that a winglet has on the global circulation strength is not the same for all wing incidence values. For the case shown, the winglet apparently decreases the circulation strength at zero wing incidence but increases it at the other two angles. Examination of the full data set for this case reveals that the winglet tip vortex is the dominant vortex in the system at zero incidence. When the incidence is increased to three degrees, however, the vortex trailed from the wing/winglet junction becomes dominant. This trend continues with increasing incidence as can be observed in Fig. 7. Clearly, there is a complex relationship between these two vortex systems that depends on the twist distribution and cant angle of the winglet.
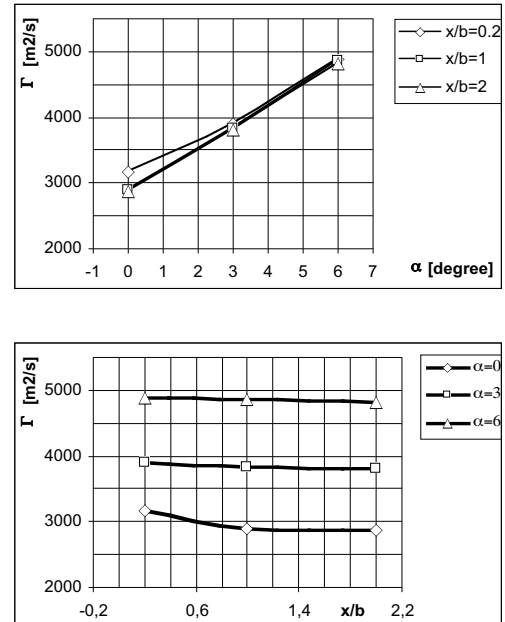
Fig. 13. Circulation behind wing tip model A as a function of wing incidence and downstream distance
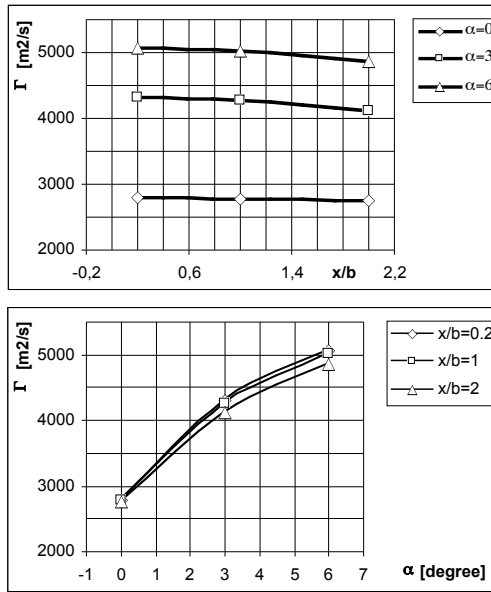
Fig. 14. Circulation behind wing tip model B as a function of wing incidence and downstream distance

The results of Tables 1 and 2 are summarised in Figs. 13 and 14 where the average values of circulation for the two wing tip models are plotted as a function of wing incidence and downstream distance. The direct proportionality between circulation and lift would suggest that, for the incidence range considered here, the circulation would vary linearly with incidence. In fact, this is true for the basic wing tip (wing tip model A). Even in this case, however, there is some deviation from this at the x/b=0.2 location for α=0$^{\rm o}$. The reason for this is not immediately obvious but could possibly be associated with the three-dimensionality of the vortex roll-up process.

The results for wing tip model B, Fig. 14, do not exhibit the linearity with incidence of those of the other wing tip. These results are, as discussed previously, a consequence of the complex interaction between the main wing and winglet flows and, in particular, the relationship between the winglet tip vortex and the wing/winglet junction vortex.

Vortex theory suggests that the intensity of circulation in an ideal flow field will remain constant regardless of downstream distance. In reality, the circulation reduces as the vortex structures progress downstream because of viscous dissipation. The range of downstream distance covered by the present measurements is quite restricted but, nevertheless, all of the data exhibit varying decays in circulation strength with downstream distance.

4.4.3 Downstream Wake Analysis

Using the information presented in Figs. 8 and 9 it is possible to chart the vertical movement of the wake of the main wing with downstream distance. This information is compared for the two wing tip models in Fig. 15. The measurements clearly show that the downward convection of the wing wake is significantly reduced when the winglet is installed (model B). In fact, the wake trajectory for model B at an incidence of six degrees is equivalent to the wake trajectory for model A at three degrees. This behaviour is consistent with a reduction in the downwash from the tip vortex system when the winglet is installed and will inevitably impact on the induced drag of the wing. Any reduction in the induced drag has to be considered together with any increase in drag associated with the additional wing area of the winglet. These effects play off against each other to determine the overall benefit, or otherwise, of the winglet.
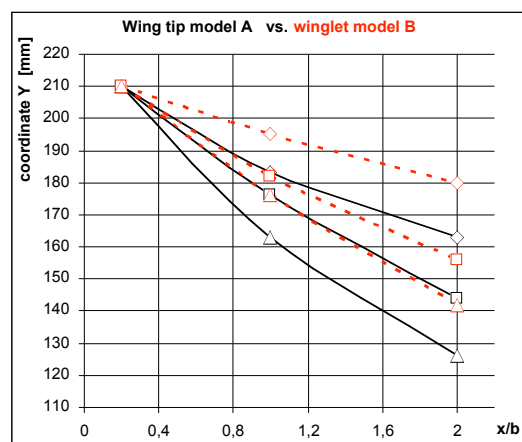
Fig. 15. Downstream wake positions (vertical) behind wing tip model A and wing tip model B

5 Conclusion

Results have been presented of hot-wire measurements behind two wing tip models; one a basic wing tip and the other incorporating a winglet. It has been shown that, for the same wing incidence, the wing tips produce vortex systems of approximately equivalent circulation strength. There are, however, some differences that can be attributed to the additional contribution of the winglet itself. This contribution has been found to be incidence dependent.

Although the effect of the winglet on the overall circulation strength is relatively small, its effect on the local downwash in the vicinity of the wing tip is much more marked. The winglet significantly reduces the downwash and will have a beneficial impact on the induced drag. This, however, has to considered in light of any increase in drag arising from the increase in overall wing area.

References

[1] Volkers DF. *Improving Aerodynamic Characteristics by means of Turbulence Management: A Fokker View*. 1st edition, The Lpswisch Book Company, 1996.

[2] Jarvis J, Selberg B. Investigation of Aerodynamic Improvements Using Wing Tip Sails. *3 7th AIAA Aerospace Sciences Meeting and Exhibit*, Reno, NV, AIAA 99-0530, January 1999

[3] Patterson J C. Wingtip Vortex Turbine. United States Patent # 4,917,332, April 17, 1991

[4] Snyder M H. Effects of a Wingtip-Mounted propeller on Wing Lift, Induced Drag, and Shed Vortex Pattern. Aeronautical Report 68-5, Department of aeronautical Engineering, Wichita State University, December 1968

[5] Allen J G. Vortex Drag Reduction Using Wing Tip Sails Thesis. Cranfield Institute of Technology, Bedford, England, 1976

[6] La Roche U, Palffy S. WING-GRID, a Novel Device for Reduction of Induced Drag on Wings. *Proceedings ICAS 96*, Sorrento, September 1996

[7] Lanchester, F W. *Aerodynamics*. Constable & Co, London, 1907

[8] Prandtl, L. Theory of lifting Surfaces. NACA TN9, 1920

[9] Whitcomb, R T. A Design Approach and Selected Wind-Tunnel Result at High Subsonic Speed for Wing-Tip Mounted Winglets. NASA TN D-8260, July 1976

[10] Marsden, D J. Winglets for Sailplanes. *Technical Soaring*, Volume 15, No. 4, October 1991